Computational Mechanics 32 (2003) 291–300 © Springer-Verlag 2003
DOI 10.1007/s00466-003-0486-4

Preliminary results on acoustic modelling of cavitating propellers

F. Salvatore, S. Ianniello

Abstract The numerical prediction of the acoustic pressure field induced by cavitating marine propellers is addressed. A hydrodynamic model for transient sheet cavitation on propellers in non–uniform inviscid flow is coupled with a hydroacoustic model based on the Ffowcs Williams–Hawkings equation. The proposed hydroacoustic approach, novel to marine applications, allows to split the noise signature into thickness and loading term contributions. Both hydrodynamic and hydroacoustic model equations are solved via boundary integral formulations. Numerical predictions of the propeller noise by using the Ffowcs Williams–Hawkings equation are compared to those obtained by a classical Bernoulli equation approach. The influence of cavitation on the noise waveforms is discussed by comparing non–cavitating and cavitating propeller flow results.

Keywords Marine propellers, Boundary Integral Methods, Ffowcs Williams–Hawkings Equation, Cavitation, Acoustic analogy

1 Introduction

Cavitation is one of the major constraints in marine propeller design. Among cavitation detrimental effects, vibrations and noise generated by transient blade cavities on propellers in the wake of a ship hull are of primary importance. Experimental observations show that unsteady cavitation–induced pressure pulses may be largely higher than those measured under non–cavitating flow conditions, whereas noise spectra exhibit significant harmonics at multiples of the blade frequency. Theoretical investigations of the hydroacoustics of cavitating propellers are typically performed under inviscid–flow assumptions by determining the pressure from the potential velocity field by means of the Bernoulli theorem (here referred to as the Bernoulli equation model, e.g., [1]).

F. Salvatore (✉), S. Ianniello
INSEAN - Italian Ship Model Basin,
Via di Vallerano, 139, 00128 Rome,
Italy
E-mail: f.salvatore@insean.it

The authors wish to thank Prof. S.A. Kinnas for providing a detailed documentation of the experiment used as the test case in the present analysis. The present work was supported by the *Ministero dei Trasporti e della Navigazione* in the frame of INSEAN Research Program 2000–02.

The aim of the present paper is the theoretical prediction of the acoustic pressure field induced by marine propellers by using a coupled hydrodynamics/hydroacoustics analysis based on a boundary element methodology. The hydroacoustic model is based on the Ffowcs Williams–Hawkings (FWH) equation [3]. This may be considered as an extension of the early Lighthill equation [8], accounting for the basic mechanisms of noise generation related to the shape of the body and the loads it experiences along its motion through the fluid. The FHW equation represents a standard solving approach for aeroacoustics problems, whereas, to the authors' knowledge, no application to the analysis of marine propellers is documented in the literature.

A characterizing feature of the FWH equation is that the noise signature is split into three different components: thickness, loading and quadrupole noise. The last term is important only for high tip speed blades and has been extensively treated by the second author for the analysis of helicopter rotors at high transonic regime [4, 5]. For incompressible flow analyses, only thickness and loading terms are considered. In particular, the influence of the cavity on both thickness and loading noise components may be investigated.

The FWH equation model requires as input the pressure distribution over the propeller surface and the cavity thickness distribution during a revolution. Numerical predictions are obtained through the so-called Formulation 1A developed by Farassat [2], a procedure widely used for linear aeroacoustic analyses of helicopter rotors. The thickness noise is assumed to be originated by step-by-step shape variations of a *virtual* blade, *i.e.*, a blade whose shape is modified to include the transient cavity, while the loading noise component is related to blade load fluctuations.

The hydroacoustic model above is coupled with a hydrodynamic model based on a boundary integral formulation for the analysis of incompressible inviscid flows around lifting bodies [10]. The approach is applied here to the analysis of an isolated propeller in a prescribed non uniform inflow (behind–hull operating conditions). Unsteady propeller cavitation is studied by using a nonlinear sheet cavity model derived from [7] and [6]. The resulting approach is valid for leading edge cavitation attached to the blade suction side (partial sheet cavitation). The cavity trailing edge region is modelled via a closed–cavity scheme and the cavity shape is determined by a free–cavity length iterative approach.

For the sake of completeness, only a brief outline of both hydrodynamics and hydroacoustics models is given

in the following sections, whereas the reader is referred to cited references for details. A preliminary validation of the proposed coupled hydrodynamic/hydroacoustic methodology is presented and numerical results are compared to those obtained by using the Bernoulli equation model.

2 Hydrodynamic analysis

Basic assumptions in the present hydrodynamics formulation are that the unperturbed flow is incompressible and inviscid. In addition, the perturbation velocity field $\mathbf{v}$ induced by the propeller is assumed to be irrotational and hence it can be expressed in terms of a scalar potential as $\mathbf{v} = \nabla\varphi$. In a frame of reference $(Oxyz)$ fixed to the propeller, with the x-axis aligned to the propeller axis and downstream pointing, the unperturbed flow velocity is $\mathbf{v}_I = \mathbf{v}_A + \mathbf{\Omega} \times \mathbf{x}$, where $\mathbf{v}_A$ is the incoming flow velocity in the propeller disk plane (prescribed, in the present analysis), and $\mathbf{\Omega} = 2\pi n \mathbf{e}_x$ is the propeller angular velocity. Thus, the total velocity field in the rotating frame is

$$\mathbf{q} = \mathbf{v}_I + \nabla\varphi \ . \tag{1}$$

The pressure p is given by the Bernoulli equation that, in the rotating frame, reads

$$\frac{\partial\varphi}{\partial t} + \frac{1}{2}q^2 + \frac{p}{\rho_0} + gz_0 = \frac{1}{2}v_I^2 + \frac{p_0}{\rho_0} \ , \tag{2}$$

where $q = \|\mathbf{q}\|, v_I = \|\mathbf{v}_I\|, p_0$ is the ambient pressure, ρ_0 is the fluid density, g is the gravity acceleration and z_0 denotes depth.

By incompressible flow assumptions, the potential φ satisfies the Laplace equation $\nabla^2\varphi = 0$ in the fluid region $\mathscr{V}_P$ limited by the propeller surface, by the trailing wake and by the cavity surface. In the framework of potential flow modelling of lifting bodies, the trailing wake denotes a zero thickness layer where the vorticity generated on the body is shed, and represents a discontinuity surface for the potential. The cavity denotes the fluid region where high–speed vaporization occurs. In the present approach the cavity is assumed to be a confined in a thin layer attached to the blade suction side.

The Laplace equation for φ is solved by imposing boundary conditions on $\partial\mathscr{V}_P$. On the wetted (*i.e.*, cavitation–free) portion $\mathscr{S}_{WB}$ of the propeller surface $\mathscr{S}_B$, the impermeability condition yields $\mathbf{q}\cdot\mathbf{n} = 0$, or, recalling Eq. (1)

$$\frac{\partial\varphi}{\partial n} = -\mathbf{v}_I \cdot \mathbf{n} \quad \text{on } \mathscr{S}_{WB} \ , \tag{3}$$

where $\mathbf{n}$ is the outward unit normal to the surface.

Across the wake surface $\mathscr{S}_W$ the pressure is continuous. By applying mass and momentum conservation laws under non cavitating flow conditions, yields $\Delta(\partial\varphi/\partial n) = 0$, where Δ denotes discontinuity across the two sides of the wake surface. Combining these wake conditions and the Bernoulli equation (2), one obtains that the potential discontinuity $\Delta\varphi$ is convected along wake streamlines, and the convection velocity is the averaged flow velocity on both sides of $\mathscr{S}_W$,

$$\Delta\varphi(\mathbf{x}, t) = \Delta\varphi(\mathbf{x}_{TE}, t - \tau_W) \quad \text{on } \mathscr{S}_W \ , \tag{4}$$

where $\mathbf{x}_{TE}$ is the trailing edge wake point lying on the same streamline as $\mathbf{x}$, and τ_W is the convection time from $\mathbf{x}_{TE}$ to $\mathbf{x}$. A further condition on φ is required in order to assure that no finite pressure jump may exist at the body trailing edge (Kutta condition). Following [10], this is equivalent to impose $\Delta\varphi(\mathbf{x}_{TE}) = \varphi^u_{TE} - \varphi^l_{TE}$, where φ^u_{TE} and φ^l_{TE} denote, respectively, suction and pressure side blade trailing edge potentials. In order to take into proper account crossflow effects, the Kutta condition is enforced by means of a pressure–based iterative approach.

Boundary conditions on the cavity surface $\mathscr{S}_C$ are imposed by assuming that the cavity is a fluid region where the pressure is constant and equal to the vapor pressure p_v. By imposing $p = p_v$ on $\mathscr{S}_C$, and by using the Bernoulli equation (2), results

$$q = \left[(nD)^2\sigma_n - 2\left(\frac{\partial\varphi}{\partial t} + gz_0\right) + v_I^2\right]^{\frac{1}{2}}, \quad \text{on } \mathscr{S}_C \ , \tag{5}$$

where $\sigma_n = (p_0 - p_v)/\frac{1}{2}\rho_0(nD)^2$ denotes the cavitation number referred to the propeller rotational speed n and diameter D. Equation (5) is used to obtain a Dirichlet–type condition for φ on $\mathscr{S}_C$ in terms of σ_n. By introducing on $\mathscr{S}_C$ a curvilinear coordinate system with s, u, archlengths in, respectively, chordwise and spanwise directions, and by recalling Eq. (1), one obtains a non linear condition for φ of the type

$$\varphi(s,u) = \varphi(s_{CLE},u) + \int_{s_{CLE}}^{s} \mathscr{F}\left(q, \frac{\partial\varphi}{\partial u}, \frac{\partial\varphi}{\partial n}, \mathbf{v}_I\right) \mathrm{d}\tilde{s} \quad \text{on } \mathscr{S}_C \ , \tag{6}$$

where s_{CLE} is the cavity leading edge abscissa. A detailed derivation of Eq. (6) and the expression of function $\mathscr{F}$ may be found, *e.g.*, in [6].

The condition $p = p_v$ and hence Eqs. (5) and(6) are not valid in the aft portion of the cavity where pressure tends to wetted flow conditions through complex two–phase flow phenomena. In the present approach, a cavity–closure region is introduced in which pressure is forced to vary smoothly from $p = p_v$ to wetted flow values behind the cavity trailing edge.

An expression of the cavity thickness h_c is obtained by imposing a non–penetration condition on $\mathscr{S}_C$. By combining the constant–pressure and the impermeability conditions, yields that $\mathscr{S}_C$ is a material surface. Denoting by $\mathscr{S}_{CB}$ the cavitating portion of $\mathscr{S}_B$, and by η the normal distance to $\mathscr{S}_{CB}$, the above condition corresponds to $(\partial/\partial t + \mathbf{q}\cdot\nabla)(\eta - h_c)$, or

$$\frac{\partial h_c}{\partial t} + \mathbf{q}\cdot\nabla_S h_c = \frac{\partial\varphi}{\partial n} + \mathbf{v}_I\cdot\mathbf{n} \quad \text{on } \mathscr{S}_{CB} \ , \tag{7}$$

where ∇_S denotes the surface gradient on $\mathscr{S}_{CB}$. Equation (7) represents a partial differential equation for h_c that may be solved once $\varphi, \partial\varphi/\partial n$ and $\partial\varphi/\partial t$ on $\mathscr{S}_{CB}$ are known.

The Laplace equation for the velocity potential is solved here by means of a boundary integral formulation. By

assuming that the perturbation vanishes at infinity, the third Green identity yields at any point $\mathbf{x} \in \mathscr{V}_P$

$$E(\mathbf{x})\varphi(\mathbf{x}) = \oint_{\hat{\mathscr{S}}_B} \left(\frac{\partial \varphi}{\partial n} G - \varphi \frac{\partial G}{\partial n}\right) \mathrm{d}\mathscr{S}(\mathbf{y}) - \int_{\mathscr{S}_W} \Delta\varphi \frac{\partial G}{\partial n} \mathrm{d}\mathscr{S}(\mathbf{y}) \ , \tag{8}$$

where $\hat{\mathscr{S}}_B = \mathscr{S}_{WB} \cup \mathscr{S}_C$, $G = -1/4\pi\|\mathbf{x} - \mathbf{y}\|$ is the Green's function of the Laplace equation in an unbounded three-dimensional domain, and E equals $0, 1/2, 1$, respectively, inside, on, or outside $\partial\mathscr{V}_P$.

In the case $\mathbf{x} \in \hat{\mathscr{S}}_B$, the numerical solution of Eq. (8) determines φ on $\mathscr{S}_{WB}$ and $\partial\varphi/\partial n$ on $\mathscr{S}_C$ once $\partial\varphi/\partial n$ on $\mathscr{S}_{WB}$ is given by Eq. (3), $\Delta\varphi$ on the wake is given by Eq. (4) combined with the Kutta condition, whereas φ on $\mathscr{S}_C$ is given by Eq. (6). Equation (8) is solved by using a boundary element approach. The potential–flow boundary surfaces are divided into hyperboloidal quadrilateral elements. Equation (8) in discretized form is enforced at each surface element centroid on $\mathscr{S}_B$. Flow quantities are assumed to be constant on each element. Influence coefficients in the discretized form of Eq. (8) are computed by using analytical integration as proposed in [10].

In the present analysis, the wake surface $\mathscr{S}_W$ is assumed to be an helical surface with a prescribed pitch distribution. At the trailing edge, $\mathscr{S}_W$ is tangent to the blade suction side, whereas downstream the propeller, the wake pitch is determined as an average between the hydrodynamic pitch of the unperturbed inflow and the blade pitch angle.

The shape of the cavity is unknown *a priori* and is determined via an iterative procedure. First, in solving Eq. (8), the surface $\mathscr{S}_C$ is replaced by the cavitating portion of the blade surface $\mathscr{S}_{CB}$. This approximation is justified by experimental evidences that a sheet cavity thickness is usually very thin as compared to propeller dimensions, and prevents additional computational effort required by surface re–gridding and influence coefficients re–computing during the cavity shape updating process. At each time step, $\mathscr{S}_{CB}$ is guessed and Eq. (8) is solved. Once the potential field on $\mathscr{S}_{CB}$ is known, Eq. (7) is used to determine the cavity thickness. By this, a new estimate of $\mathscr{S}_{CB}$ is obtained by using a free–cavity length approach, as described in [12]. This process is repeated until convergence of predicted cavity planform and volume.

3
Hydroacoustic analysis

3.1
Ffowcs Williams–Hawkings equation model

The theoretical basis for the analysis of sound generated by a body moving in a fluid is represented by the Ffowcs Williams–Hawkings equation, which can be derived from the basic conservation laws of mass and momentum written in terms of generalized functions. This way, a discontinuity in the flow variables is allowed, representing the jump of flow quantities across the moving body surface. By neglecting viscosity effects (the fluid-body dynamic interaction is described by the scalar pressure field on the body surface) and by assuming that the fluid is compressible and undergoes transformations with negligible entropy changes (the pressure–density relationship can be approximated by the linear term of its series expansion, *i.e.* $p' = c_0^2\tilde{\rho}$, where c_0 is the sound speed, $\tilde{\rho}$ the density perturbation field and p' denotes the acoustic pressure disturbance), the FWH equation reads

$$c_0^2 \bar{\Box}^2 \tilde{\rho} = \bar{\Box}^2 p' = \frac{\bar{\partial}}{\partial t}[\rho_0 v_n \delta(f)] - \nabla \cdot [p\delta(f)\mathbf{n}] + \nabla : [H(f)\mathbf{T}] \ , \tag{9}$$

where $v_n = -\mathbf{v}_I \cdot \mathbf{n}$, an overbar denotes a generalized derivative, the D'Alambert operator has been defined as

$$\bar{\Box}^2 = \frac{1}{c_0^2}\frac{\bar{\partial}^2}{\partial t^2} - \bar{\nabla}^2 \ , \tag{10}$$

and the Lighthill stress tensor is expressed by $\mathbf{T} = \rho\mathbf{v} \otimes \mathbf{v} + (p - c_0^2\tilde{\rho})\mathbf{I}$. In equation (9) the body surface is described by $f(\mathbf{x}, t) = 0$, with $f > 0$ outside the body; inside the body ($f < 0$) the following assumptions hold, concerning field density, pressure and velocity, respectively: $\rho = \rho_0, p = p_0, \mathbf{v} = 0$. Moreover, $f(\mathbf{x}, t)$ is defined so as to make $|\nabla f| = 1$ on $f = 0$, and hence $\nabla f = \mathbf{n}$.

The three source terms appearing in Eq. (9) are known as *thickness* (monopole), *loading* (dipole) and *quadrupole* terms. Thickness contribution is related to the body geometry and kinematics, while the loading noise concerns the load distribution upon the blade, and hence implicitly includes the effect of the propeller wake. Noise contribution from the flow field surrounding the body is included in the quadrupole source term: it accounts for turbulence, mutual interactions between the hull wake and the propeller, and high speed flow effects as in the case of shock waves occurrence.

The numerical solution of the FWH equation can be achieved through the use of the Green's function technique, which turns equation (9) into an integral form. The linear terms are represented by some surface integrals and are generally computed with an integration upon the blade surface, exploiting the knowledge of the body shape and motion and the pressure distribution during the revolution period. On the contrary, the evaluation of the quadrupole source term requires the knowledge of the fluid velocity field around the body and can be very complex to achieve because of the shock delocalization phenomena and the non-compactness of the supersonic sources [4]. In this context we will avoid to treat the numerical solution of the nonlinear terms, since the usual operating condition of a marine propeller definitely removes any problem concerning the shock waves and the nonlinearities of interest are *only* related to the turbulence and the mutual interactions between the propeller and the hull wake.

Following a standard Green function approach, Eq. (9) may be suitably managed in order to obtain the following integral expressions for thickness and loading acoustic pressure terms, respectively:

$$4\pi p_T(\mathbf{x},t) = \oint_{\mathscr{S}} \left[\frac{\rho_0 \dot{v}_n}{r|1-M_r|^2}\right]_{\tau^*} \mathrm{d}\mathscr{S}(\mathbf{y}) + \oint_{\mathscr{S}} \left[\frac{\rho_0 v_n \left(r\dot{\mathbf{M}}\cdot\hat{\mathbf{r}} + c_0 M_r - c_0 M^2\right)}{r^2|1-M_r|^3}\right]_{\tau^*} \mathrm{d}\mathscr{S}(\mathbf{y}) \quad ; \quad (11)$$

$$4\pi p_L(\mathbf{x},t) = \frac{1}{c_0}\oint_{\mathscr{S}} \left[\frac{(\dot{p}\cos\theta + p\dot{\mathbf{n}}\cdot\hat{\mathbf{r}})}{r|1-M_r|^2}\right]_{\tau^*} \mathrm{d}S + \oint_{\mathscr{S}} \left[p\frac{\cos\theta - M_n}{r^2|1-M_r|^2}\right]_{\tau^*} \mathrm{d}\mathscr{S}(\mathbf{y}) + \frac{1}{c_0}\oint_{\mathscr{S}} \left[\frac{p\cos\theta}{r^2|1-M_r|^3}\left(r\dot{\mathbf{M}}\cdot\hat{\mathbf{r}} + c_0 M_r - c_0 M^2\right)\right]_{\tau^*} \mathrm{d}\mathscr{S}(\mathbf{y}) \quad (12)$$

where the symbol $(\dot{\cdot})$ denotes time derivation. The overall acoustic pressure is then obtained as

$$p' = p_T + p_L \quad (13)$$

Within Eqs. (11) and (12), the integration domain $\mathscr{S}$ denotes the surface of the *source*, which in the present analysis corresponds to the propeller blade under non cavitating conditions, and to the blade plus the bubble when cavitation occurs ($\mathscr{S} = \hat{\mathscr{S}}_B$, see Eq. (8)). The quantity r denotes the source–observer distance, whereas θ is the angle between $\hat{\mathbf{r}}$ (the unit vector along the source-observer direction) and the unit vector normal to $\mathscr{S}$. In addition, a Mach vector $\mathbf{M} = -\mathbf{v}_I/c_0$ is introduced, whereas $M = \|\mathbf{M}\|$, $M_r = \mathbf{M}\cdot\hat{\mathbf{r}}$, and $M_n = \mathbf{M}\cdot\mathbf{n}$.

This particular representation of the FWH linear terms is known as the Farassat *Formulation 1A* [2], and is widely used in the aeronautical context. The subscript τ^* indicates that for each source point all of the kernel quantities must be evaluated at the emission time, which represents, given the observer time t and location $\mathbf{x}$, the instant when the contribution to the noise signature was released. The determination of τ^* represents the *core* of the numerical algorithm and is achieved with an iterative procedure, solving the equation:

$$\tau = t - \frac{r}{c_0} = t - \frac{|\mathbf{x} - \mathbf{y}(\eta,\tau)|}{c_0} = \Phi(\tau) \quad , \quad (14)$$

where $\mathbf{x}$ and $\mathbf{y}$ represent the *present* and the *retarted* observer and source point positions, respectively, and η is the coordinate-vector of source point in the body frame of reference. Starting from the initial time $\tau = t$ and the corresponding positive value $f(\tau) = r/c_0$, the research for the root of the function $f(\tau) = [\tau - \Phi(\tau)]$ proceeds backwards, with a prescribed time step $\Delta\tau$, up to the first sign inversion; then, the emission time τ^* is captured by subsequent iterations through the typical bisection method until a specified error condition is satisfied. Nevertheless, the occurrence of a cavitation bubble upon the blade corresponds to a change of the body geometry during the revolution period and the location of each source point cannot be determined analitically. Then the algorithm requires a set of angular positions of the *actual* source (blade plus cavity) in input to evaluate the retarded quantities through a suitable interpolation procedure.

It is worthwhile to mention that for marine propeller applications, the velocity $\mathbf{v}$ is very small as compared to the sound speed c_0, and hence the Mach number $\mathbf{M}$ is close to zero; in addition, the emission time delay in Eq. (14) is also close to zero because of the c_0 value in water. Thus, results by the present approach are fully comparable with those obtained by a classical approach based on potential velocity equation (8) and the Bernoulli equation (2) combined (see next section), where the incompressible flow assumption is explicit. The accuracy of numerical solutions by Eqs. (11) and (12) is not affected by the order of magnitude of both c_0 and $\mathbf{M}$.

3.2 Bernoulli equation model

For comparison purposes, a conventional hydroacoustic approach based on the Bernoulli equation (2) to determine the pressure from the velocity potential is also described. Equation (8) is used to evaluate the potential at an arbitrary location $\mathbf{x}_a$ immersed into the fluid domain (*i.e.*, acoustic observer location). Specifically, once φ and $\partial\varphi/\partial n$ on $\hat{\mathscr{S}}_B$ are known, Eq. (8) with $E(\mathbf{x}_a) = 1$ provides an explicit representation of $\varphi_a = \varphi(\mathbf{x}_a)$. In the case of an observer that translates with the propeller advance speed $\mathbf{v}_0 = v_0\mathbf{e}_x$, Eq. (2) with term gz_0 neglected, yields

$$p = p_0 - \rho_0\left(\frac{\partial\varphi_a}{\partial t} + v_0\frac{\partial\varphi_a}{\partial x} + \frac{1}{2}|\nabla\varphi_a|^2\right) \quad . \quad (15)$$

The perturbation velocity $\nabla\varphi_a$ in the right hand side of Eq. (15) is evaluated here through a boundary integral representation by taking the gradient of Eq. (8).

By the present approach, it is not possible to separate loading and thickness contributions to the pressure. Nevertheless, the effect of the unsteady cavitation may be isolated by means of an approximated derivation. To this purpose, compare Eqs. (3) and (7). A cavity sheet over the blade surface affects the potential field through an additional source distribution (hereafter referred to as the *cavity source sheet*) having intensity $\chi_{css} = \partial h_c/\partial t + \mathbf{q}\cdot\nabla_S h_c$, on $\mathscr{S}_{CB}$ and $\chi_{css} = 0$ on the cavitation–free propeller surface. The perturbation potential induced by the monopole distribution χ_{css} is

$$\varphi_{css}(\mathbf{x}) = \oint_{\mathscr{S}_B}\left(\frac{\partial h_c}{\partial t} + \mathbf{q}\cdot\nabla h_c\right) G\,\mathrm{d}\mathscr{S}(\mathbf{y}) \quad . \quad (16)$$

Next, the pressure field p_{css} is obtained by Eq. (15), with φ_a replaced by φ_{css} from Eq. (16).

By comparing Eqs. (8) and(16), follows that φ_{css} provides an approximation of the difference between velocity potential values under cavitating and non cavitating flow conditions. Moreover, p_{css} has the physical meaning of the acoustic perturbation associated to a cavity–induced equivalent source distribution on $\mathscr{S}_B$.

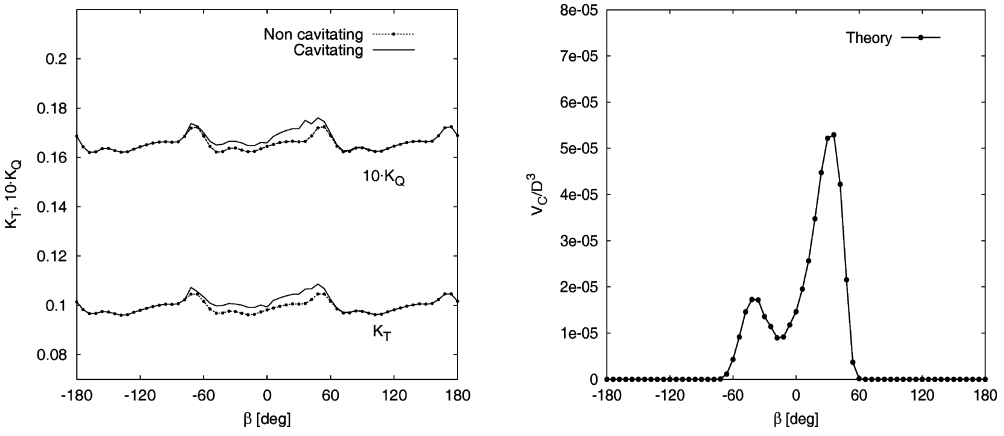

Fig. 1. Left: predicted thrust and torque coefficients K_T, K_Q during a revolution under non–cavitating and cavitating flow conditions. Right: time history of the cavity volume V_c

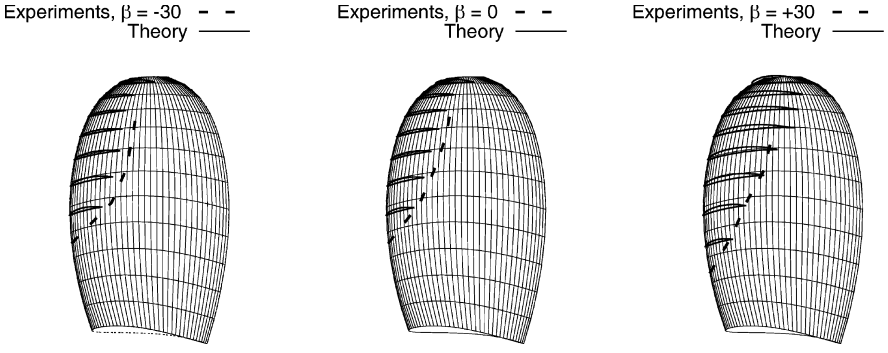

Fig. 2. Cavity patterns on the blade at three angular positions. Cavity sectional profiles predicted by the present hydrodynamic model and observed cavity trailing edge line from [9]

Table 1. Location of the considered acoustic pressure measurement points (hydrophones)

Hydroph.	x/D	y/D	z/D
1	0.00	0.66	0.00
2	0.00	2.00	0.00
3	2.00	1.50	0.00
4	−2.00	1.50	0.00

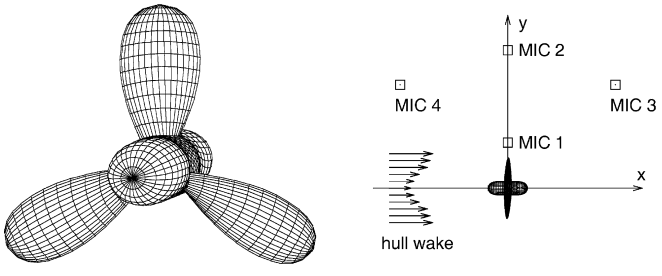

Fig. 3. Computational grid on the DTRC 4148 propeller and hydrophones location

4
Numerical results

A preliminary validation of the proposed hydroacoustic methodology is presented here by considering an isolated propeller in non uniform inflow. The selected test case is derived from flowfield measurements performed at the MIT cavitation water tunnel [9]. The DTRC 4148 three–bladed model propeller in a screen generated non axisymmetric inflow is considered. Propeller diameter, advance speed and rotational speed are, respectively, $D = 0.305$ m, $v_0 = 4.775$m/s, $n = 17.17$ rps, and hence the corresponding advance coefficient is $J = v_0/nD = 0.91$.[1] The nominal inflow to the propeller, modified to include both inflow/propeller and tunnel/propeller interactions, is considered here as an input to the numerical analysis. Both non–cavitating flow conditions and cavitating flow conditions at $\sigma_n = 2.757$ are considered here.

First, the hydrodynamic analysis is briefly addressed. Numerical investigations have been performed by discretizing each blade surface into 36 elements in chordwise direction (from leading edge to trailing edge) and 12 elements in spanwise direction, whereas 60 elements are used in the streamwise direction on each wake turn, and 816 elements are used on the hub surface. As shown in[12], a spatial discretization of this type allows to obtain negligible discretization errors. The unsteady flow under non uniform inflow conditions is analysed by discretizing each propeller revolution into 60 time steps.

Left Fig. 1 shows predicted propeller thrust coefficient $K_T = T/\rho_0 n^2 D^4$ and torque coefficient $K_Q = Q/\rho_0 n^2 D^5$ during a revolution. The abscissa β represents the angular position of the reference blade, with $\beta = 0^\circ$ corresponding to the blade in the twelve o'clock position. The comparison between non–cavitating and cavitating flow conditions highlights the increase of both thrust and torque due to a blade thickening effect related to sheet cavitation. Right

[1] Numerical analysis flow conditions differ from those by experiments in order to take into account for tunnel wall effects, as discussed in[11].

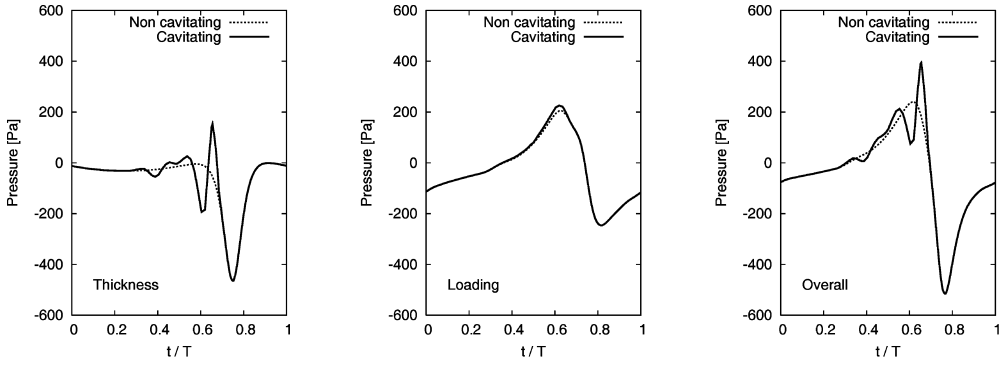

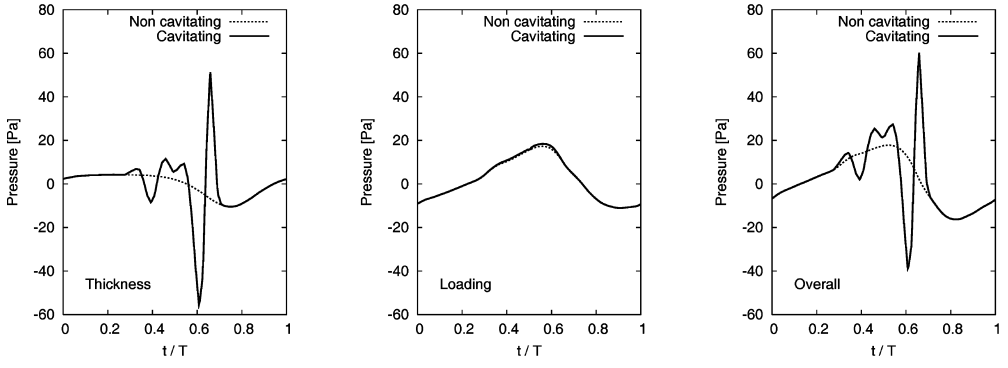

Fig. 4. Acoustic pressure signatures at hydrophone 1 (top) and 2 (bottom) by FWH equation model. Comparison between cavitating and non cavitating conditions for thickness (left), loading (center) and overall (right) noise predictions

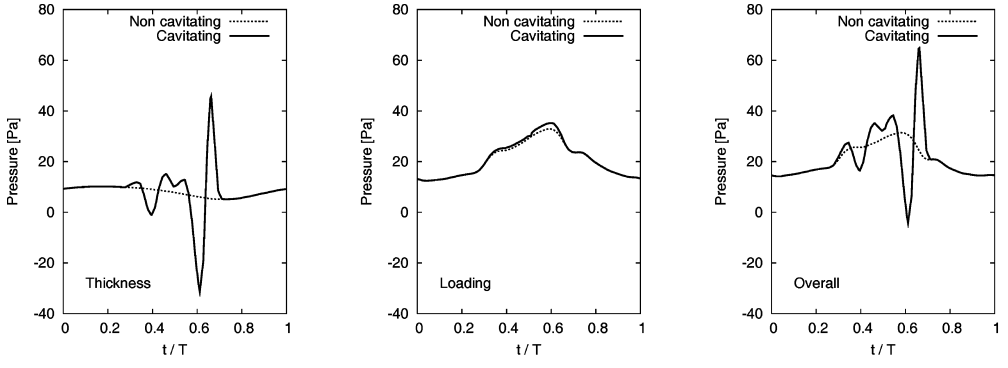

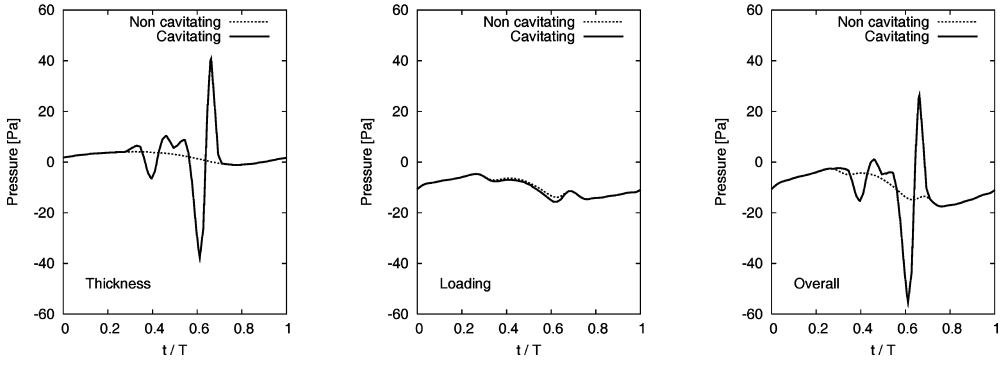

Fig. 5. Acoustic pressure signatures at hydrophone 3 (top) and 4 (bottom) by FWH equation model. Comparison between cavitating and non cavitating conditions for thickness (left), loading (center) and overall (right) noise predictions

Fig. 1 depicts the time hystory of the cavity volume V_C on a single blade during a revolution. Inception and increase of the cavity is related to low velocity inflow regions that determine a strong blade loading and hence low pressure vaporization in the leading edge suction side region. Test conditions considered in the experiment determine a two–peaks cavity volume pattern, with inception at about $\beta = -70°$ and collapse at $\beta = +60°$. Unfortunately, measured data for quantities in Fig. 1 are not available, whereas photographs of the cavity shape at several blade positions are presented in [9]. Predicted cavity shapes and observed cavity trailing edge lines are compared in Fig. 2, where three representative angular positions of the blade are considered. It may be noted that the extension of the cavity is satisfactorily captured by the present hydrodynamic model.

The hydrodynamic solution described above provides the input for the hydroacoustic analysis discussed hereafter. Four selected hydrophones are considered in and out of the propeller plane, to qualitatively appreciate some

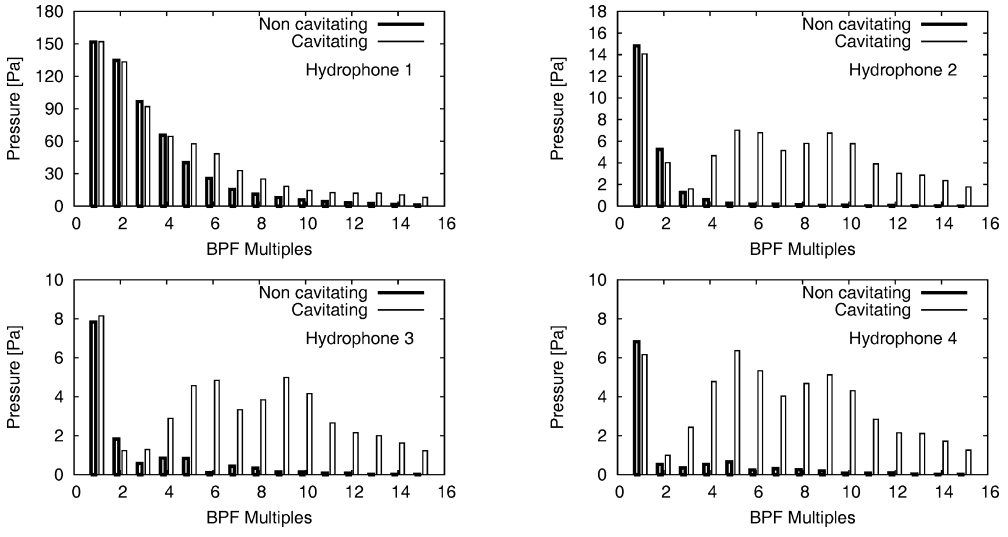

Fig. 6. Acoustic pressure spectra by the FWH equation model as a function of blade passing frequency (BPF) multiples. Comparison between cavitating and non cavitating conditions

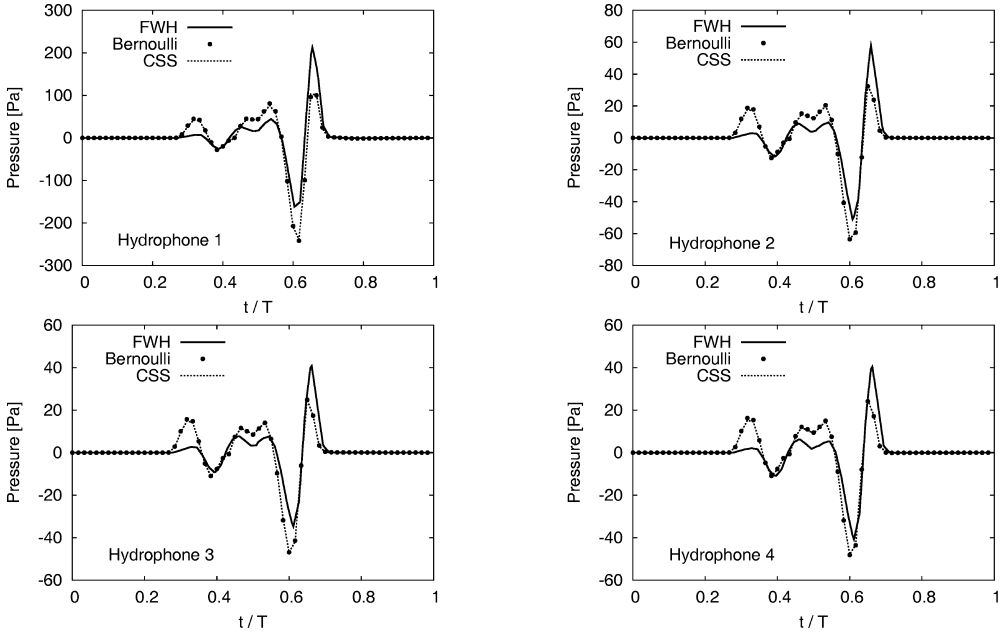

Fig. 7. Pure cavity–induced noise at hydrophones 1 to 4. Comparison between predictions by FWH equation, Bernoulli equation and by cavity source sheet (CSS) models

basic features of noise predictions by the FWH model. In fact, hydrophones 1 and 2 are located in the propeller plane where the thickness noise should be predominant, whereas hydrophones 3 and 4 are positioned downstream and upstream, respectively, the propeller disk plane: at these locations a significant contribution from the loading term is expected. Coordinates of the four hydrophone locations are given in Table 1. Figure 3 depicts the computational grid on the DTRC 4148 propeller and the hydrophone locations.

The present hydrodynamic solution is determined on the actual three-bladed model (thus accounting for the mutual inteference between the blades), whereas, the acoustic pressure signatures determined by considering only single blade perturbation are presented and discussed hereafter. This allows to better appreciate the influence of sheet cavitation on the resulting noise waveform and to compare the numerical results at different operating conditions. By flow periodicity, the overall acoustic pressure may be simply obtained by superimposing shifted signatures from each blade.

Figure 4 shows noise time hystories predicted by the FWH approach at the two in plane locations: hydrophones 1 (top pictures) and 2 (bottom pictures). Noise amplitude is plotted as a function of the time t/T, where $T = 1/n$ denotes the propeller revolution period, and $t = 0$ corresponds to the reference blade at $\beta = -180°$. At each location the comparison between cavitating and non cavitating flow conditions is presented.

Specifically, thickness noise components p_T from Eq. (11) are shown in the left Fig. 4, loading term components p_L from Eq. (12) are shown in center Fig. 4, and the overall noise signature $p_T + p_L$ is reported in the right Fig. 4. Looking at the non cavitating results at hydrophone 1 (very close to the blade tip) the noise signatures are exactly the expected ones: at in plane locations the thickness noise exhibits a symmetrical shape and the highest (negative) peak value of the acoustic pressure, while the loading term

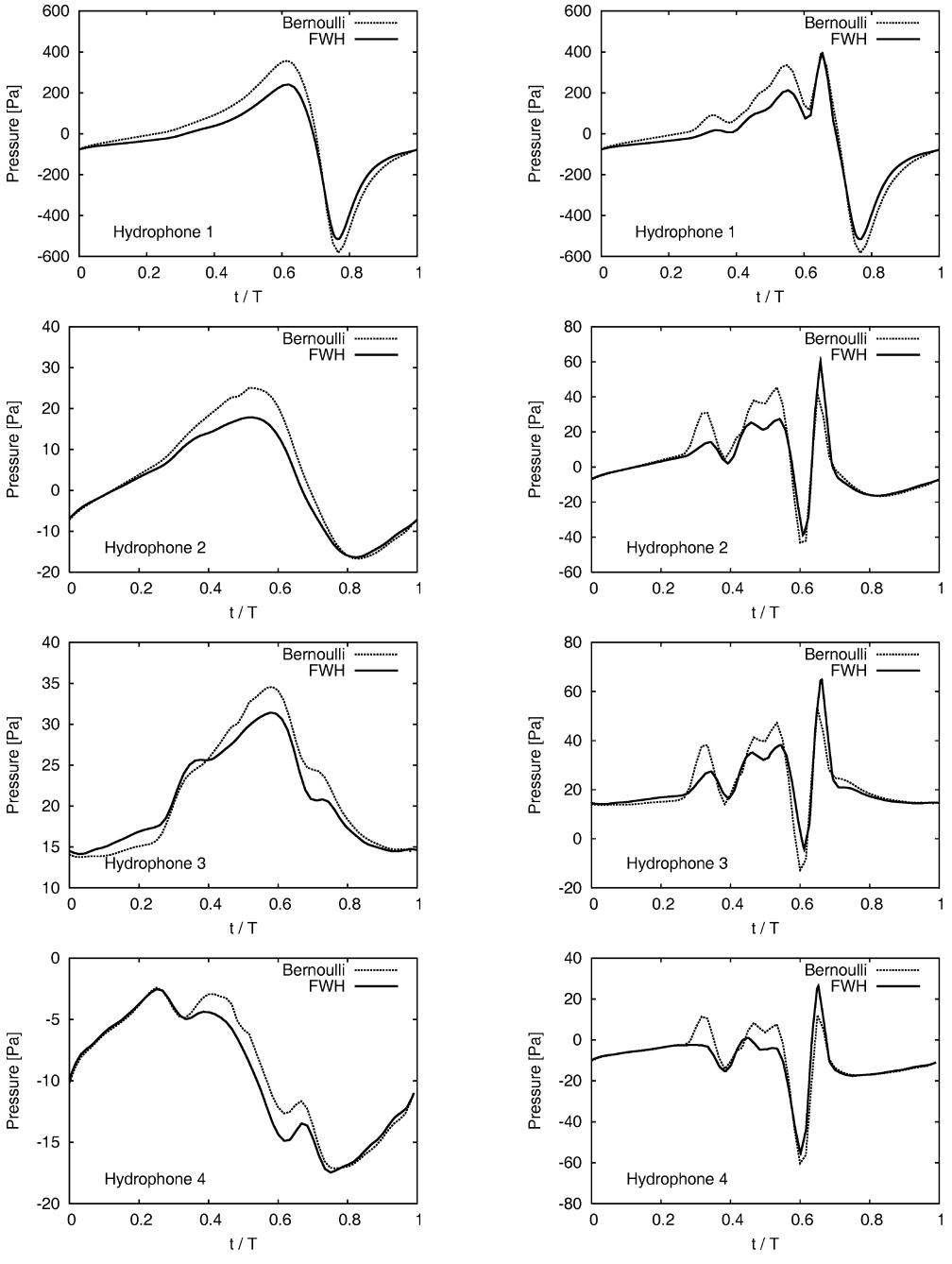

Fig. 8. Comparison between overall noise by FWH equation model and by Bernoulli equation model in non–cavitating (left) and in cavitating (right) flow conditions. Observers 1 to 4 are shown from top to bottom

has a typical waveform with some slightly smaller peak values: in practice, the resulting signatures are very similar to those of an aeronautical propeller rotating at subsonic speed. The most relevant differences at cavitating conditions arise from the monopole term: the occurrence of sheet cavitation corresponds to a more impulsive character of the noise waveform and some higher frequency components appear. On the contrary, the dipole contribution seems to be not altered by vaporization, but a little increase in the pressure at the angular positions affected by the cavity. Moving far from the blade tip (hydrophone 2) the thickness contribution is still comparable with the loading term (as order of magnitude) but rapidly decreases and the percentage difference between cavitating and non cavitating flow has a remarkable increase. The cavitation influence on the loading noise is still negligible, but the effect on the monopole term becomes really notable and heavily affect the overall noise signature.

These features become even more evident by moving far from the propeller disk plane, as shown in Fig. 5 where results at hydrophones 3 and 4 are reported. Out of plane the loading term is predominant with respect to the thickness noise contribution generated by the (non cavitating) blade, but the occurrence of the sheet bubble deeply changes the resulting noise waveform. Due to the symmetrical location of these hydrophones with respect to the propeller plane, the thickness component at non cavitating condition is practically the same, while the loading term rightly exhibits the sign inversion due to pressure values on face and back sides of the blade. Nonetheless, a very similar thickness noise waveform arises at the two different positions also at cavitating condition, eventhough the presence of the vapour

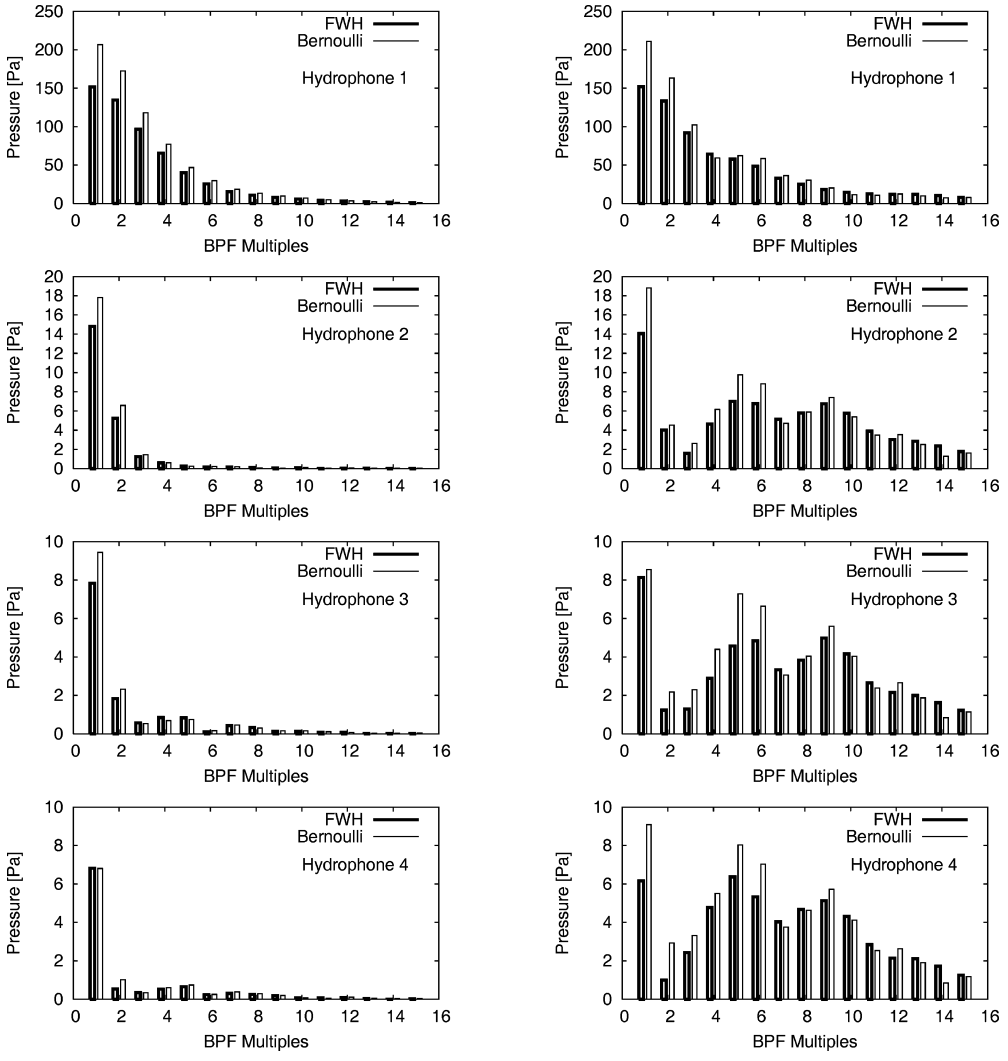

Fig. 9. Acoustic pressure spectra as a function of blade passing frequency (BPF) multiples. Comparison between FWH equation model and Bernoulli equation model results at non–cavitating (left) and at cavitating (right) flow conditions. Observers 1 to 4 are shown from top to bottom

sheet is limited to the upper surface of the blade; this result points out the actual *monopole* behaviour of the bubble, which acts as a pulsating sphere with a 3D homogeneous influence around the body.

Noise predictions via the FWH equation confirm the monopole character of sheet cavity–generated sound. The negligible influence on the loading noise component is reasonable, since the pressure time histories of each source point is not heavily affected by the occurrence of cavitation. On the contrary, *source-body* (blade plus vapour sheet) geometry and the corresponding normal velocity to the body surface rapidly change during the revolution period, thus explaining the higher frequency content and the impulsive character of the resulting noise signatures.

The above considerations are confirmed by considering non cavitating and cavitating overall acoustic pressure spectra, as shown by Fig. 6, where tonal components are plotted as a function of multiples of blade passing frequency. The intensity of tonal components is given here as $A_i = \sqrt{c_i^2 + s_i^2}$, where c_i, s_i are, respectively, cosine and sine terms of the Fourier series. At hydrophone 1, the noise spectrum is not heavily affected by the occurrence of cavitation due to the small distance of the hydrophone with respect to the propeller; by increasing the distance from the propeller (locations 2 to 4) a relevant higher–frequency content is observed as a consequence of sheet cavitation as the dominating noise generation mechanism.

The monopole character of cavitating propeller noise may be further observed by comparing Fig. 7 the *pure* cavitation effects on the overall noise signature as determined by the FWH solver, the Bernoulli equation model and the cavity source sheet (CSS) model (see subsect. 3.2). Specifically, curves labelled as 'FWH' and 'Bernoulli' represent the difference between non cavitating and cavitating acoustic pressure, whereas the CSS acoustic pressure is obtained by combining Eq. (16) and Eq. (15) with φ_a replaced by φ_{css}. It may be observed a good agreement among the three different prediction approaches. Moreover, all of them highlight the impressive similarities of the cavity (monopole) effect all around the propeller. This is particularly evident looking at hydrophone 1 results: close to the blade tip the shape of the noise signature is primarily determined by the body thickness and loading terms (top Fig. 4), but the cavity contribution is substantially the same.

Finally, Fig. 8 focus on the comparison between non cavitating and cavitating overall acoustic pressure time histories by the FWH equation and the Bernoulli equation models. From a qualitative point of view the agreement between the two hydroacoustic models is very satisfactory:

the resulting noise signatures are very similar in shape and order of magnitude both at cavitating and non cavitating condition, thus providing substantially the same evaluation of the sheet cavitation influence on the overall noise.

The above considerations are confirmed by Fig. 9, where noise tonal components are plotted as a function of multiples of blade passing frequency.

5 Conclusions

A boundary element methodology for a coupled hydrodynamic/hydroacoustic analysis of cavitating marine propellers in non uniform flow has been presented. The hydrodynamic analysis is based on a standard inviscid–flow sheet cavitation model. The hydroacoustic model is based on the Ffowcs Williams–Hawkings equation, a well known methodology for aeronautical applications that is totally neglected in marine propeller problems.

Work described in the present paper represents the first step towards a thorough investigation of FWH equation capability to predict cavitating propellers noise. Some basic features of the cavitating flow noise radiation are highlighted. The vapour sheet behaves as a monopole term, with a homogeneous, three dimensional sound radiation around the propeller. The thickness noise contribution assumes an impulsive waveform with high frequency components, whereas the loading term is just slightly affected by the transient cavity and the overall noise signature exhibits a notable increase in the far field.

Noise predictions by the FWH equation are in satisfactorily agreement with those obtained by using the Bernoulli equation: the waveform of signatures are fully comparable and both the two models point out the major features of cavitation induced noise generation. However, some discrepancies between numerical results by the two approaches are present even at non cavitating flow conditions and require further investigations.

References

1. **Breslin JP, van Houten RJ, Kerwin JE, Johnsson CA** (1982) Theoretical and Experimental Propeller–Induced Hull Pressures Arising from Intermittent Blade Cavitation, Loading and Thickness. Transactions SNAME 90: 111–151
2. **Farassat F** (1981) Linear acoustic formulas for calculation of rotating blade noise. AIAA J. 19 (9): 1122–1130
3. **Ffowcs Williams JE, Hawkings DL** (1969) Sound generation by turbulence and surfaces in arbitrary motion. Philosophical Transactions of the Royal Society A264: 321–342
4. **Ianniello S** (1999) Quadrupole noise predictions through the FW–H equation. AIAA J. 37 (9): 1040–1047
5. **Ianniello S** (1999) Algorithm to integrate the Ffowcs Williams–Hawkings equation on supersonic rotating domain. AIAA J. 37 (9): 1048–1054
6. **Kinnas SA, Fine NE** (1992) A nonlinear boundary element method for the analysis of unsteady propeller sheet cavitation. Proceedings of the Nineteenth ONR Symposium on Naval Hydrodynamics, Seoul (Korea), pp. 717–737
7. **Lee JT** (1987) A Potential Based Panel Method for the Analysis of Marine Propellers in Steady Flow, Report 87–13, Dept. of Ocean Engineering, MIT
8. **Lighthill MJ** (1952) On Sound Generated Aerodynamically. Proceedings of the Royal Society. A11, pp. 564–587
9. **Mishima S, Kinnas SA, Egnor D** (1995) The CAvitating PRopeller EXperiment (CAPREX) Phases I & II, Technical Report. Dept. of Ocean Engineering, MIT
10. **Morino L, Chen LT, Suciu E** (1975) Steady and oscillatory subsonic and supersonic aerodynamics around complex configurations. AIAA J. 13: 368–374
11. **Mueller AC, Kinnas SA** (1997) Cavitation predictions using a panel method. Proc. of the ASME Symposium on Marine Hydrodynamics and Ocean Engineering, Dallas (USA), Vol. 14, pp. 127–137
12. **Pereira F, Salvatore F, Di Felice F, Elefante M** (2002) Experimantal and Numerical Investigation of the Cavitation Pattern on a Marine Propeller. Proceedings of the Twenty-Fourth ONR Symposium on Naval Hydrodynamics, Fukuoka (Japan)